Supporting Information

Wang et al. 10.1073/pnas.1800907115

SI Methods

Purification, Crystallization, and Structure Determination. The expression and purification of hP2X3 ΔN5ΔC33-T13P/S15V/V16I, referred to as hP2X3-MFCslow, were performed as described previously (1). For crystallization, 1 μL of hP2X3-MFCslow at 2 mg/mL and 0.2 mM AF-219 were mixed with 1 μL of the reservoir solution (0.05 M $MgCl_2$, 0.1 M Glycine pH 9.0, and 22 to 24% PEG 400) and crystallized by vapor diffusion method over the reservoir resolution. Crystals grew after 2 wk to 3 wk, and were harvested with cryoprotectant solution (0.05 M $MgCl_2$, 0.1 M Glycine pH 9.0, 40% PEG 400). After flash-cooling in liquid nitrogen, the crystals were subjected to X-ray diffraction. The X-ray diffraction data were collected at the SPring-8 beamline BL41XU and processed using XDS (2). The AF-219-bound hP2X3 structure was solved by molecular replacement with Phaser, using the *apo* state structure of hP2X3 (PDB ID code 5SVJ) as the template. The model building was performed using COOT (3), and the structure was refined using PHENIX (4). Data collection and refinement statistics are shown in Table S1.

Molecular and Cell Biology. The hP2X3 plasmid was purchased from Open Biosystems. All mutations were made using QuikChange mutagenesis kit and then confirmed by DNA sequencing. WT and mutant plasmids were transfected into HEK-293 cells with Hilymax (Dojindo Laboratories) according to the manufacturer's instructions. HEK-293 cells were cultured in Dulbecco's Modified Eagle's medium (Gibco), supplemented with 10% FBS (Gibco), in a 37 °C incubator with 95% air and 5% CO_2. PPADS, suramin, RO-3, RO-51, and TC-P 262 were purchased from Tocris. All other drugs were purchased from Sigma-Aldrich.

Patch Clamp Recording. All electrophysiology recordings were performed 24 h to 48 h after transfection using Axon 200B at the room temperature. The holding potential was −60 mV. Patch electrodes had resistance ranging from 3 MΩ to 5 MΩ when filled with intracellular solution containing 120 mM KCl, 30 mM NaCl, 1 mM $MgCl_2$, 0.1 mM $CaCl_2$, and 5 mM EGTA (pH 7.2 adjusted by Tris-base). Cells were bathed in a standard extracellular solution containing 150 mM NaCl, 5 mM KCl, 10 mM glucose, 2 mM $CaCl_2$, 1 mM $MgCl_2$, and 10 mM Hepes (pH 7.4 adjusted by Tris-base). Data were sampled at 10 kHz and filtered at 2 kHz. To prevent run-down of the ATP-evoked currents, nystatin-perforated patch clamp technique was used (5, 6), with the application intervals of ATP set to about 10 min. However, run-up and run-down still occurred occasionally. To avoid the influence by run-down and run-up, recordings were discarded when current amplitudes in response to the first two ATP applications varied more than 15%. For statistical analysis, data were normalized to the average value of the first two ATP-evoked currents. All antagonists of hP2X3 were preapplied for 2 min and then coapplied in the presence of the agonist. NPM was diluted to 1 mM and immediately perfused to the cell membrane for 5 min.

Homology Modeling, in Silico Docking, and Dynamics Simulations. Due to the absence of the structural information for the LF domain in the crystal structure of hP2X3 at the *apo* state (PDB ID code 5SVJ) (1), this disorder region in the crystal structure was filled in by using homology modeling with the program MODELER (7). The resulting models were further optimized by 1.2-ns MD simulations (8, 9). AF-353 and other P2X3 antagonists were docked into corresponding sites with the program Induce-Fit-Docking using default parameters (10). MD simulations were performed and results were further analyzed using the program DESMOND according to previous description (5, 11). The binding site cavity in hP2X3 at the *apo* or open state, or the AF-219-bound state, was defined by using an "eraser" algorithm based on the shape of the receptors (12). For hP2X3 in complex with AF-219, the AF-219 within hP2X3 was separated before the cavity definition was carried out in receptors.

Well-Tempered Metadynamics. Metadynamics is a technique in which the potential for one or more chosen variables is modified by periodically adding a repulsive potential of Gaussian shape at the location given by particular values of the variable (13). As we previously described (5), metadynamics simulations were carried out using DESMOND (5). Before doing metadynamics simulations, the complex between P2X3 and AF-353 was equilibrated by 1.2-ns MD simulations under NPT conditions at 1 atm and 320 K using the OPLS2005 of the all-atom force field, as implemented in DESMOND. All simulations were carried out in a solvent and in cubic periodic boundary conditions.

The estimation $F(s, t)$ at time t of the free-energy surfaces $F(s)$ as a function of the CVs was determined by metadynamics in newly developed well-tempered variant (14, 15), using the following equation (14, 15):

$$F(s,t) = -\frac{T+\Delta T}{\Delta T}V(s,t)$$

where $V(s, t)$ is the bias potential added to the system and T is the temperature of the simulation. ΔT is the difference between the temperature of the CV and the temperature of the simulation. The bias potential is made up by the sum of the Gaussians deposited along the trajectories of the CVs. This approach can increase barrier crossing and facilitate the exploration in the CVs' space by tuning ΔT (14, 15). A Gaussian deposition rate of 1.3 $kcal{\cdot}mol^{-1}{\cdot}ps^{-1}$ was initially used and gradually decreased on the basis of the adaptive bias with a ΔT of 2,400 K.

Chemical Synthesis of AF-219.

The 2-isopropyl-4-methoxyphenol. To a solution of 1-(2-hydroxy-5-methoxyphenyl)ethan-1-one (1 g, 6.02 mmol) in tetrahydrofuran (THF, 10 mL) was added methylmagnesium chloride (3 mL, 3.0 M solution in THF) at 0 °C. The reaction mixture was stirred at room temperature until completion, and water (30 mL) was added into the mixture. Then the mixture was adjusted to pH 6 using 2 N HCl. The aqueous layer was extracted with EtOAc (3 × 10 mL). The combined organic layers were washed with brine, dried over anhydrous Na_2SO_4, filtered, and concentrated in vacuo.

To the residue dissolved in THF (10 mL) was added 6M HCl (1 mL) and 10% Pd/C (0.1 g). The reaction mixture was stirred at room temperature under H_2 atmospheric pressure until the TLC indicated the consumption of starting materials. The reaction mixture was filtered through celite, and the insoluble substance was washed with THF. The filtrate was concentrated in vacuo to give 2-isopropyl-4-methoxyphenol (0.85 g, 85% yield for two steps) as colorless oil; ^{1}H NMR (300 MHz, $CDCl_3$) δ 6.82 (d, J = 2.8 Hz, 1H), 6.72 (d, J = 8.6 Hz, 1H), 6.65 (d, J = 2.7 Hz, 1H), 3.80 (s, 3H), 3.23 (dt, J = 13.7, 6.9 Hz, 1H), 1.29 (s, 3H), 1.27 (s, 3H). Electrospray ionization mass spectrometer (ESI MS) m/z = 165.1 $[M - H]^-$.

The 2-(2-isopropyl-4-methoxyphenoxy) acetonitrile. To a solution of 2-isopropyl-4-methoxyphenol (0.5 g, 3.0 mmol) in *N*,*N*-dimethylformamide (DMF) (5 mL) was added iodoacetonitrile (0.5 g,

3.0 mmol) and K_2CO_3 (414 mg, 3.0 mmol). The reaction mixture was stirred at room temperature until completion, and water (30 mL) was added into the mixture. The aqueous layer was extracted with EtOAc (3 × 5 mL). The combined organic layers were washed with brine, dried over anhydrous Na_2SO_4, filtered, and concentrated in vacuo. The residue was purified by flash chromatography to give 2-(2-isopropyl-4-methoxyphenoxy) acetonitrile (467 mg, 76% yield) as yellow oil; ^{1}H NMR (300 MHz, $CDCl_3$) δ 6.91 (d, J = 8.8 Hz, 1H), 6.86 (d, J = 2.8 Hz, 1H), 6.73 (dd, J = 8.8, 3.0 Hz, 1H), 4.76 (s, 2H), 3.82 (s, 3H), 3.30 (dt, J = 13.8, 6.9 Hz, 1H), 1.26 (s, 3H), 1.23 (s, 3H). ESI MS m/z = 228.1 $[M + Na]^+$.

The 5-(2-isopropyl-4-methoxyphenoxy)pyrimidine-2,4-diamine. To a solution of 2-(2-isopropyl-4-methoxyphenoxy)acetonitrile (0.3 g, 1.46 mmol) in DMF (3 mL) was added tert-butoxy bis(dimethylamino)methane (255 mg, 1.46 mmol). The reaction mixture was stirred at 110 °C until completion, and aniline hydrochloride (189 mg, 1.46 mmol) was added into the reaction mixture. Then the reaction mixture was stirred at 120 °C until completion, and guanidine carbonate (265 mg, 2.19 mmol) was added into the reaction mixture. The reaction mixture was stirred at 120 °C until completion, and water (20 mL) was added into the mixture. The aqueous layer was extracted with EtOAc (3 × 5 mL). The combined organic layers were washed with brine, dried over anhydrous Na_2SO_4, filtered, and concentrated in vacuo. The residue was purified by flash chromatography to give 5-(2-isopropyl-4-methoxyphenoxy)pyrimidine-2,4-diamine (172 mg, 43% yield for three steps) as white solid; ^{1}H NMR (300 MHz, DMSO-d6) δ 7.21 (s, 1H), 6.80 (d, J = 2.8 Hz, 1H), 6.67 (dd, J = 8.9, 2.9 Hz, 1H), 6.60 (d, J = 8.8 Hz, 1H), 6.27 (brs, 2H), 5.71 (brs, 2H), 3.68 (s, 3H), 3.28 to 3.23 (m, 1H), 1.19 (s, 3H), 1.17 (s, 3H). ESI MS m/z = 275.1 $[M + H]^+$.

The 5-((2,4-diaminopyrimidin-5-yl)oxy)-4-isopropyl-2-methoxybenzenesulfonamide (AF-219). To a solution of 5-(2-isopropyl-4-methoxyphenoxy) pyrimidine-2,4-diamine (40 mg, 0.15 mmol) in chlorosulfonic acid (0.3 mL) was added phosphorus oxychloride (0.5 mL). The reaction mixture was stirred at 75 °C for 6 h, and then concentrated in vacuo. Ammonia (0.5 mL, 7.0 mol/L in MeOH) was added into the mixture, which was stirred at room temperature for 2 h. Water (3 mL) was added into the reaction mixture, which was then filtered to give 5-((2,4-diaminopyrimidin-5-yl)oxy)-4-isopropyl-2-methoxybenzenesulfonamide (48 mg, 94% yield) as white solid; ^{1}H NMR (300 MHz, DMSO-d_6) δ 7.38 (s, 1H), 7.12 (s, 1H), 7.05 (s, 1H), 6.69 (brs, 2H), 6.14 (brs, 2H), 3.93 (s, 3H), 3.41 (dt, J = 13.7, 7.0 Hz, 1H), 1.31 (s, 3H), 1.29 (s, 3H). ESI MS m/z = 354.1 $[M + H]^+$.

Data Analysis. All of the electrophysiological recording data were analyzed using Clampfit 10 software (Molecular Devices). Pooled data are expressed as mean ± SEM, and statistics are analyzed using Student's t test or ANOVA, for which $^*P < 0.05$ and $^{**}P < 0.01$ were considered to have significant difference. Concentration–response data were fitted to the equation $I/I_{max} = 1/[1 + (IC_{50}/[A])^n]$, where I is the normalized current at a given concentration of the inhibitor, I_{max} is the maximum normalized current induced by the agonist (ATP), [A] is the concentration of the antagonist, IC_{50} is the antagonist concentration which is half-maximally effective, and n is the Hill coefficient.

1. Mansoor SE, et al. (2016) X-ray structures define human $P2X_3$ receptor gating cycle and antagonist action. *Nature* 538:66–71.
2. Kabsch W (2010) XDS. *Acta Crystallogr D Biol Crystallogr* 66:125–132.
3. Emsley P, Cowtan K (2004) COOT: Model-building tools for molecular graphics. *Acta Crystallogr D Biol Crystallogr* 60:2126–2132.
4. Adams PD, et al. (2010) PHENIX: A comprehensive Python-based system for macromolecular structure solution. *Acta Crystallogr D Biol Crystallogr* 66:213–221.
5. Zhao WS, et al. (2014) Relative motions between left flipper and dorsal fin domains favour P2X4 receptor activation. *Nat Commun* 5:4189.
6. Lewis CJ, Evans RJ (2000) Lack of run-down of smooth muscle P2X receptor currents recorded with the amphotericin permeabilized patch technique, physiological and pharmacological characterization of the properties of mesenteric artery P2X receptor ion channels. *Br J Pharmacol* 131:1659–1666.
7. Sali A, Blundell TL (1993) Comparative protein modelling by satisfaction of spatial restraints. *J Mol Biol* 234:779–815.
8. Yang H, et al. (2009) Inherent dynamics of the acid-sensing ion channel 1 correlates with the gating mechanism. *PLoS Biol* 7:e1000151.
9. Yang H, Yu Y, Li WG, Xu TL, Jiang H (2009) Conformational sampling on acid-sensing ion channel 1 (ASIC1): Implication for a symmetric conformation. *Cell Res* 19:1035–1037.
10. Sherman W, Day T, Jacobson MP, Friesner RA, Farid R (2006) Novel procedure for modeling ligand/receptor induced fit effects. *J Med Chem* 49:534–553.
11. Zhao WS, et al. (2016) A highly conserved salt bridge stabilizes the kinked conformation of β2,3-sheet essential for channel function of P2X4 receptors. *J Biol Chem* 291:7990–8003.
12. Venkatachalam CM, Jiang X, Oldfield T, Waldman M (2003) LigandFit: A novel method for the shape-directed rapid docking of ligands to protein active sites. *J Mol Graph Model* 21:289–307.
13. Laio A, Gervasio FL (2008) Metadynamics: A method to simulate rare events and reconstruct the free energy in biophysics, chemistry and material science. *Rep Prog Phys* 71:126601.
14. Barducci A, Bussi G, Parrinello M (2008) Well-tempered metadynamics: A smoothly converging and tunable free-energy method. *Phys Rev Lett* 100:020603.
15. Limongelli V, et al. (2010) Molecular basis of cyclooxygenase enzymes (COXs) selective inhibition. *Proc Natl Acad Sci USA* 107:5411–5416.

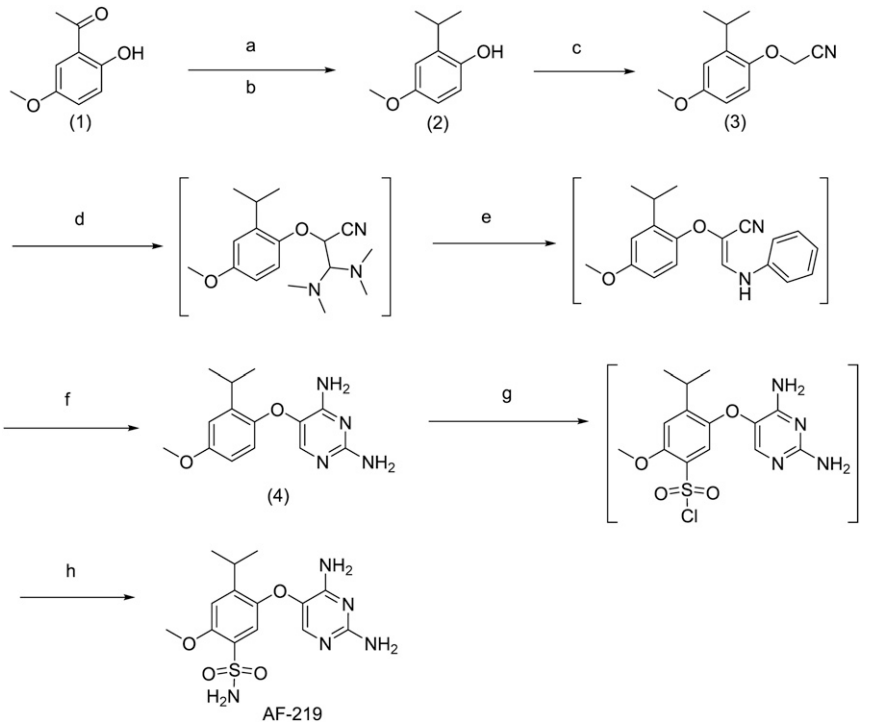

Fig. S1. Synthesis of AF-219. Reagents, conditions and yields are (step a) MeMgCl, THF, rt; (step b) H_2, Pd/C, THF, rt, 85% yield for steps a and b; (step c) ICH_2CN, K_2CO_3, DMF, rt, 76% yield; (step d) tert-Butoxy bis(dimethylamino) methane, DMF, 110 °C; (step e) aniline hydrochloride, DMF, 120 °C, and (step f) guanidine carbonate, DMF, 120 °C, 43% yield for steps d–f; (step g) $HOSO_2Cl$, $POCl_3$, 75 °C, and (step h) NH_3, rt, 94% yield for steps g and h.

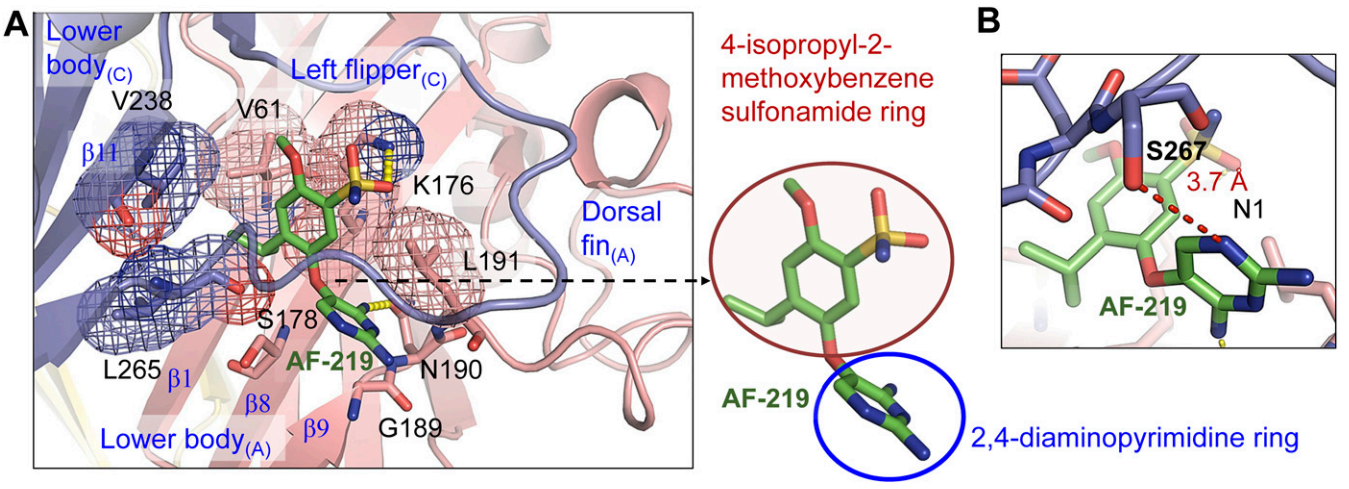

Fig. S2. A close-up view of the AF-219 binding site of hP2X3. (*A*) Zoom-in views of contacts between AF-219 and hP2X3 in the crystal structure. The key residues and AF-219 are displayed in sticks for emphasis, and mesh models were also added to residues that make hydrophobic contacts with AF-219. AF-219 was also separated from the receptor to highlight the 4-isopropyl-2-methoxybenzenesulfonamide and the 2,4-diaminopyrimidine rings. (*B*) A close-up view of the distance between AF-219 and S267. Red dotted lines indicate a distance measurement between an atom from AF-219 and one from hP2X3.

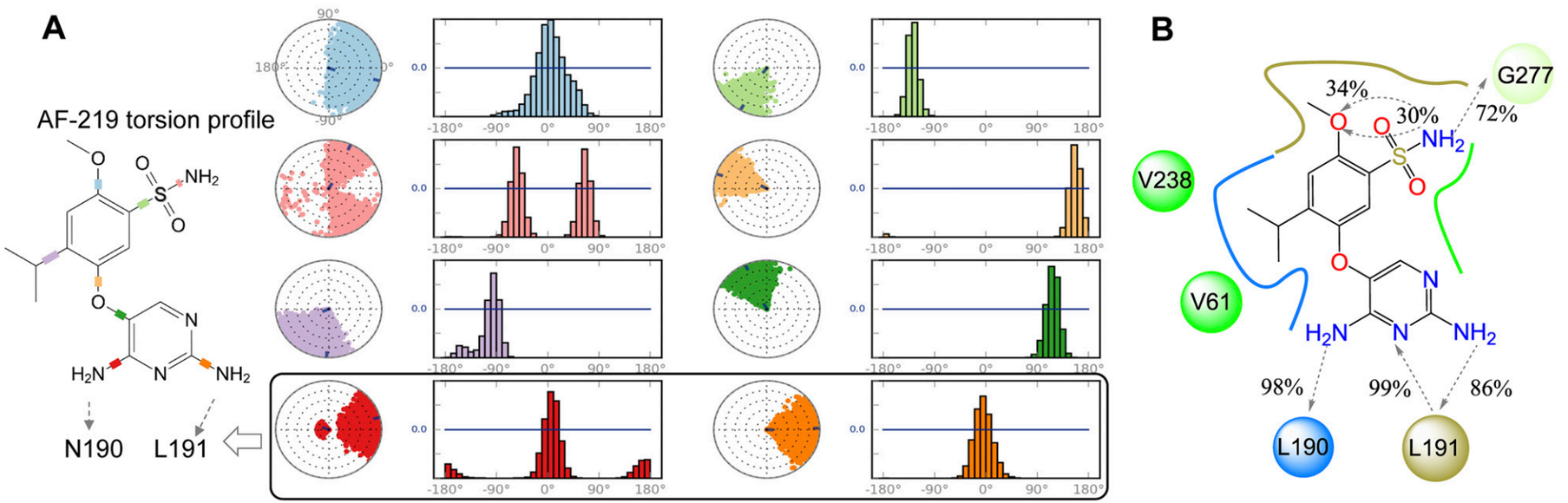

Fig. S3. Conformational evolution of every rotatable bond in AF-219 and hP2X3-AF-219 interactions throughout 300-ns MD simulations. (*A*) The AF-219 torsions plot summarizes the conformational evolution of every rotatable bond (*Left*) in AF-219 throughout the simulation trajectory (0 ns through 300.02 ns). (*Right*) The 2D schematic of AF-219 with color-coded rotatable bonds. Each rotatable bond torsion is accompanied by a radial plot (left) and bar plots of the same color (right). Radial plots describe the conformation of the torsion throughout the course of the simulation. The beginning of the simulation is in the center of the radial plot, and the time evolution is plotted radially outward. The bar plots summarize the data on the radial plots, showing the probability density of the torsion. The histogram and torsion potential relationships give insights into the conformational strain the ligand undergoes to maintain a protein-bound conformation. (*B*) A schematic of detailed AF-219 atom interactions with residues of hP2X3. Interactions that occurred more than 30% of the simulation time in the trajectory (0.0 ns through 300.02 ns) are shown.

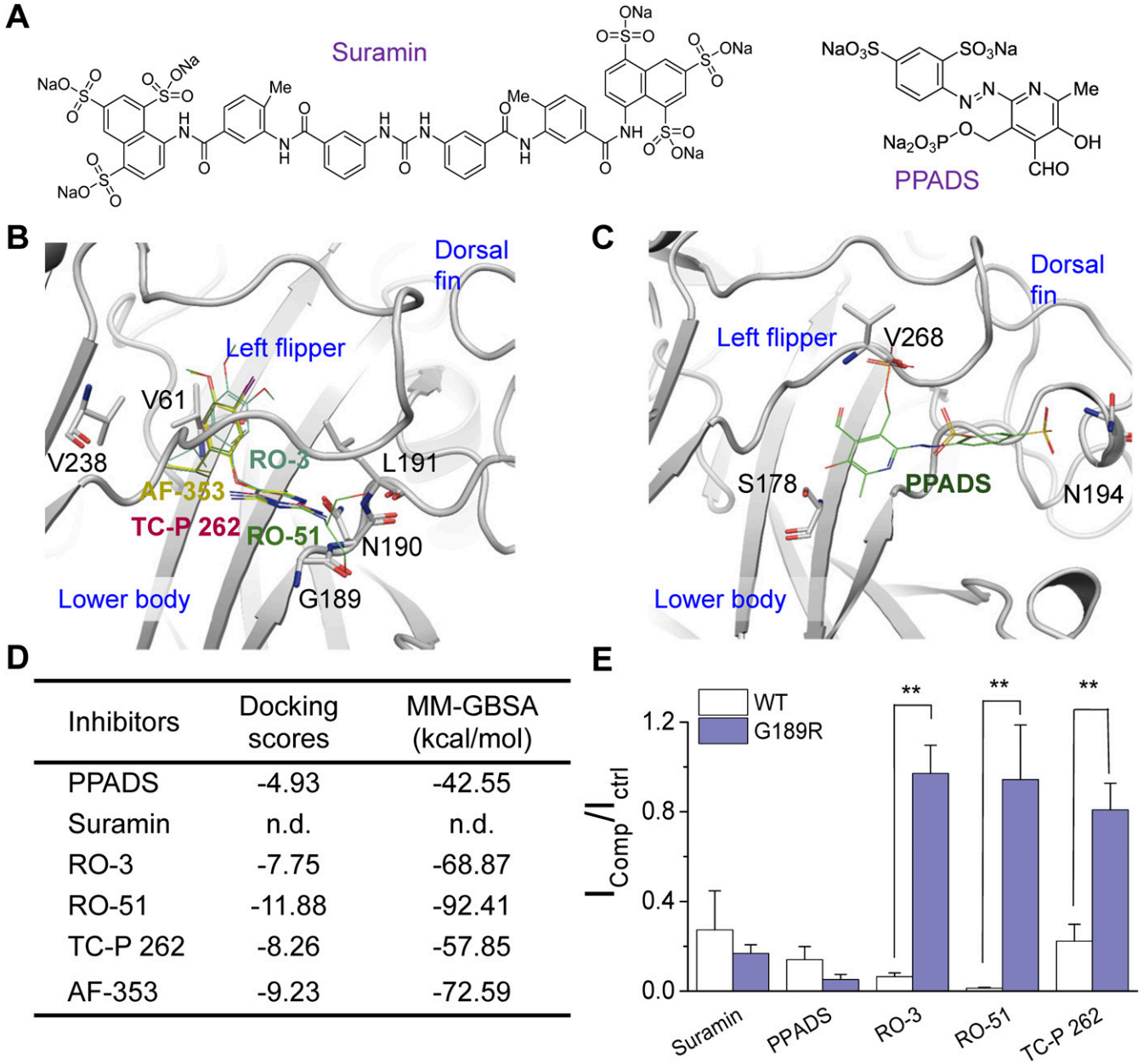

Inhibitors	Docking scores	MM-GBSA (kcal/mol)
PPADS	-4.93	-42.55
Suramin	n.d.	n.d.
RO-3	-7.75	-68.87
RO-51	-11.88	-92.41
TC-P 262	-8.26	-57.85
AF-353	-9.23	-72.59

Fig. S4. In silico docking of different P2X3 allosteric inhibitors to the identified allosteric site. (*A*) The 2D schematics of P2X3 antagonists: suramin and PPADS. (*B* and *C*) Docking poses of inhibitors using Glide. AF-353, RO-3, RO-51, and TC-P 262 (*B*) and PPADS (*C*) are in depicted in lines. (*D*) Summary of docking scores and calculated MM/GBSA binding free energy. (*E*) Summary of effects of P2X3 antagonists (suramin, 50 μM; PPADS, 50 μM; RO-3, 3 μM; RO-51, 1 μM; TC-P 262, 1 μM) on ATP (10 μM)-evoked current of hP2X3-WT and hP2X3^{G189R} (n = 3 to 4). **$P < 0.01$ vs. WT (one-way ANOVA). I_{Comp} and I_{ctrl} are peak currents in the presence and absence (control), respectively, of the antagonist.

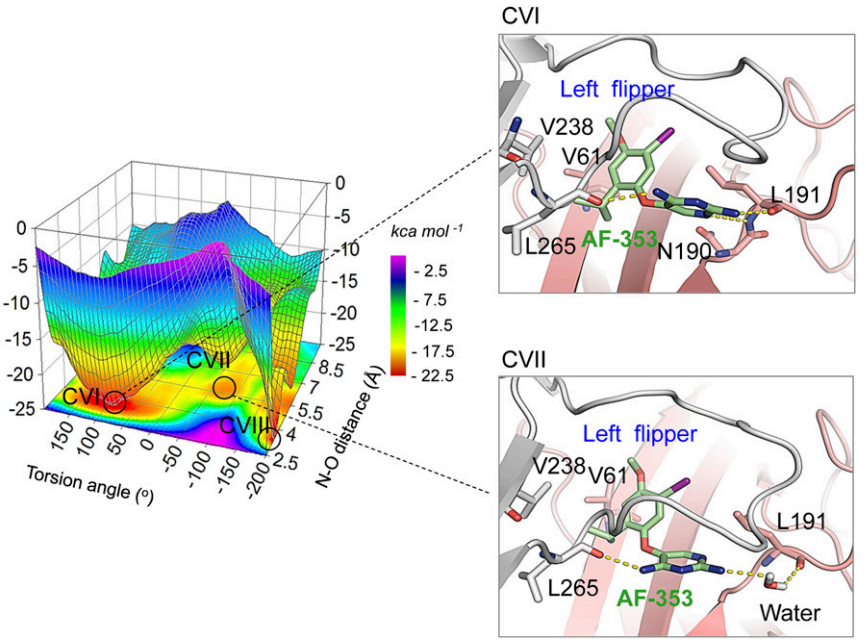

Fig. S5. Possible binding modes of AF-353 with hP2X3. Free-energy surface show the other two possible binding modes of AF-353 in hP2X3 (CVI and CVII) as determined by metadynamics simulations. The key residues and AF-353 are displayed in sticks for emphasis. Yellow dotted lines indicate H bonds between AF-353 and hP2X3.

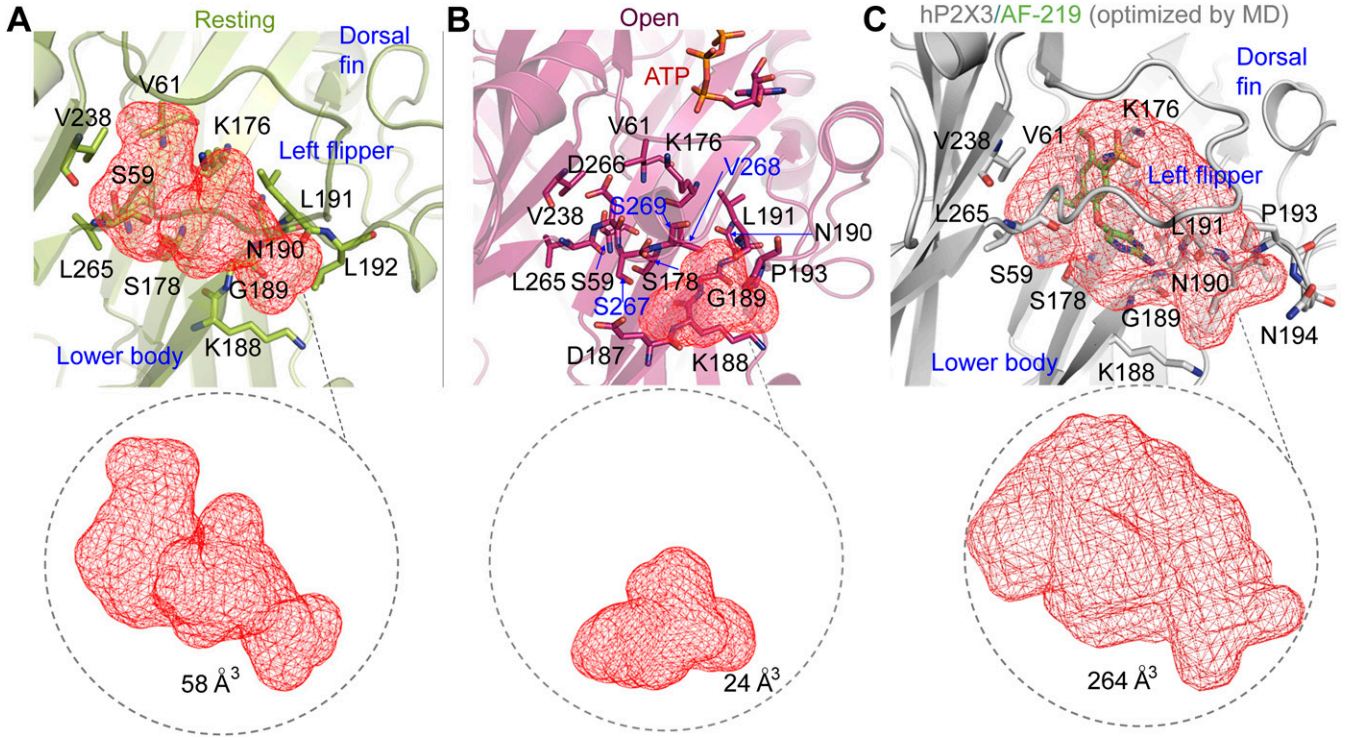

Fig. S6. The shapes and volumes of cavities fostered by the LF and LB domains of hP2X3 at *apo*, open, and AF-219 bound states. The cavities are shown as red meshes for hP2X3 at (*A*) *apo*, (*B*) open, and (*C*) AF-219-bound states. For hP2X3 bound with AF-219, the ligand and receptor molecules were separated first before the definition of the cavity was carried out in receptors. The key residues and AF-219 are displayed in sticks for emphasis.

Table S1. Data collection, phasing, and refinement statistics

Parameter	Value
Data collection	
Wavelength, Å	1.000
Space group	*H*32
Cell dimensions	
a, *b*, *c*, Å	119.6, 119.6, 235.7
α, β, γ, degrees	90, 90, 120
Resolution,* Å	50.0 to 3.40 (3.60 to 3.40)
R_{sym}*	0.070 (1.095)
$I/\sigma I$*	14.45 (1.67)
Completeness,* %	99.5 (98.2)
Redundancy*	4.9 (5.0)
$CC_{1/2}$,* %	99.9 (68.8)
Refinement	
Resolution, Å	3.4
No. reflections	17,203
R_{work}/R_{free}	23.5/29.6
No. atoms	
Protein	2,509
AF-219	24
Cations	2
B factors	
Protein	137.2
AF-219	129.6
Cations	132.4
rms deviations	
Bond lengths, Å	0.005
Bond angles, degrees	0.903
Ramachandran plot	
Favored, %	94.77
Allowed, %	5.23
Outliers, %	0

*Highest-resolution shell is shown in parentheses.